# Canadian Surveillance of Space Concept Demonstrator: Photometric Variability of Molniya-Class Objects

**Bryce Bennett**
*Royal Military College of Canada, P.O. Box 17000, Stn Forces, Kingston, ON, K7K 7B4*
**Thomas Racey**
*Royal Military College of Canada, P.O. Box 17000, Stn Forces, Kingston, ON, K7K 7B4*
**Robert Scott**
*Defence R&D Canada Ottawa, 3701 Carling Avenue, Ottawa, ON, K1A 0Z4*
**Brad Wallace**
*Defence R&D Canada Ottawa, 3701 Carling Avenue, Ottawa, ON, K1A 0Z4*

## ABSTRACT

This paper presents the results of an analysis of the time dependence of relative visible magnitudes ("light curves") of Molniya resident space objects (RSOs). The CCD image data were obtained in sidereal-stare mode, where the satellite is allowed to streak through a 'stationary' star field. Various streak extraction algorithms were coded, enabling generation and subsequent analysis of the along-track light-curves of RSOs. The algorithms were tested on virtual data, and then used to examine Molniya-class objects whose light-curves exhibit variability over the image exposure durations. Fourier analysis and other time-series comparisons were performed on archived observations made over periods ranging from a single night to more than a year. The oscillation periods appear stable over periods of up to 18 months; current data will be presented to illustrate the stability of these light curves over the past 6 years.

## 1. INTRODUCTION

The Canadian Surveillance of Space Project (SofSP) Concept Demonstrator (CD) consists of three remotely operable optical observatories constructed primarily from COTS equipment – located in Kingston, ON, Valcartier, QC, and Suffield, AB, and operated remotely from a Sensor Operations Center located in Ottawa, ON. The CD system is intended as a risk-reduction effort in advance of the launch of Sapphire, a Surveillance of Space (SofS) satellite being procured by the Canadian Department of National Defence. The CD was designed as a low cost system capable of delivering high-quality orbital metric data for deep-space objects. Metric accuracy and photometric assessments of the system have been performed showing that angular residual uncertainties were less than 3 arcseconds, with arcsecond-level biases.[1] An example of a CD telescope sensor is shown in Fig. 1.

In the sidereal tracking mode, stars appear as point sources and any object moving at a non-sidereal rate produces a 'streak' in the image. Astrometry can be done on the streak endpoints, which are time-tagged to millisecond precision by a GPS device at the CD sensor. The streak can also be analyzed to obtain a light curve using knowledge of the exposure duration and along-track CCD counts of the streak. The maximum periodicities detectable by this type of analysis are limited by the pixel-length of the satellite streak which is itself limited by relative angular speed of the object (which in turn affects the signal to noise ratio of the streak data through trailing losses), and the field of view of the camera. Further, the size of individual pixels, combined with the relative angular velocity of the object, determine the minimum period that can be detected.

The intention in performing this analysis was to explore both the observational and data-reduction issues involved in using the CD sensors as a means of obtaining and quantifying light curves for the purposes of space environment study or space object identification. With sufficient data density, the algorithms could also be employed to characterize Near Earth Objects (NEOs) or other non-resolved bodies. Eventually the algorithms may be incorporated into a suite of CD applications that includes automatic endpoint determination and photometric reduction. For this 'proof of concept' study, Molniya-class objects were chosen because: 1) at least 15 of the class are no longer attitude-controlled and exhibit cyclical brightness variations, 2) when they are in the northern sky (anywhere near the apogees of their highly inclined orbits) their line-of-sight angular rates are sufficiently low that 30 to 60 second exposures may be obtained, and 3) archived observations of sufficient exposure durations to

compare with newly acquired images of these objects exist at the Royal Military College of Canada. This paper describes the algorithm used to determine the satellite streak periodicities and compares the periodicities of several Molniya satellites from measurements taken in 2000, 2001, and 2006.

## 2. INSTRUMENTATION AND DATA

A typical CD sensor consists of a 0.35 meter, f/11 Schmidt-Cassegrain optical telescope. This study uses measurements from a variety of detectors mounted to these telescopes yielding various pixel scales. Originally, an Apogee AP7 (512x512 pixel array, 1.25 arcsec/pixel) was used in 2000; subsequently an Apogee AP8P (1024x1024, 1.25 arcsec/pixel) was installed. The most recent detector used is an Apogee Alta E42 (1024x1024 binning, 1.38 arcsec/pixel). These optics-and-camera combinations give fields of view of about 11, 21 and 24 arcminutes respectively. Data taken by these detectors is recorded in Flexible Image Transport System (FITS) format. Fig. 2 shows a typical long-exposure image delivered by a CD telescope. Note the variation in the recorded brightness of the object.

Fig. 1. Dome, and Optical Tube, Robotic Mount, and Camera Assembly of a CD Telescope

Temporal data reduction was performed on imaged streaks using a 'Space Streak Temporal Analysis Script (SSTAS) developed in MatLab. The script uses a Fourier Transform algorithm to find the frequencies exhibited in the variation of the along-track image array counts. Image file names, exposure durations, and endpoint coordinates are read into the script from an MS Excel spreadsheet. The image FITS files themselves are imported into MATLAB by the script, which can then perform calculations on the entire image to give background counts, standard deviations and variances, as well as the temporal streak analysis to be discussed in this article. The main SSTAS program was designed around a set of modular components (MatLab m-file functions) to ensure that the required algorithms could be individually tested and to ensure consistency of the subsequent analysis. Although several hundred images were examined in developing and testing the script, the conclusions presented here are based on 108 dark- and bias-frame reduced images of four Molniya objects selected for the study. The image set was restricted to: 1) those with good focus and S/N ratio, 2) images with sufficiently long exposures to show at least two complete cycles of the main period found for the object, and 3) images with well-defined endpoints. Although the data set is small, the results of this study indicate that the approach we have taken may be useful as a relatively simple means of measuring RSO periodicities.

Fig. 2. SSN#08425, Molniya 3-03, 2006 August 05, 5:46 UTC, 20 second exposure

## 3. STREAK EXTRACTION ALGORITHMS

Since the streaks can have any position angle on the CCD image, the first issue is to produce the light curve vectors (1 by N time series arrays) without loss of data quality. Since the CCD array is composed of square photon 'bins' (pixels), the streak has a temporal resolution that is limited by the pixel-length of the streak as projected onto each the CCD axes. For this reason, each space object streak is analysed by extracting two light-curves, one parallel to each of the CCD axes. For each of the two 'preferred' axial directions this procedure generates projected light-curves of various resolutions, depending on the position angle of the given streak. The extreme cases occur when a streak is parallel to one of the axes and orthogonal to the other; in such cases there is maximum temporal resolution along the one axis, and none along the other. Note that while it would be straightforward to construct an 'along-track' measure of the periodicity, the temporal resolution would be no better than this 'projection method' since (up to the 45 degree diagonal) the pixel cross-sections lengthen in proportion to the tangent of the position angle of the streak with respect to the axis – i.e. the pixel density is the same along-steak as it is along-axis.

The streak extraction procedure can be chosen for consistency with the data quality. For an exactly-focused image with optimal optics and camera, and with perfect seeing, the full width half maximum (FWHM) of the satellite streak 'width' would be on the order of a single CCD element. The streak extraction function call can be set to generate each element of the light-curve vector by simply reading the pixel counts of the pixels that form the line segment connecting the two end-points of the streak. However, this method would miss any counts in adjacent elements, and assume perfect end-point determination. Since the CD optics-and-camera configuration used for this analysis delivers images containing streaks with point spread functions (PSFs) whose FWHM are typically two or more pixels, a different approach was taken. The vector elements are generated by the weighted summation of pixel counts. For example, each vector element may be set as the sum of the 3 by 3 sub-array centred on a given array coordinate.

Fig. 3 shows an example extracted streak vector: the curves in each graph represent the resultant streak vector elements produced by four different extraction functions. The vector with the highest counts in each of the two plots is the vector produced by a 25-cell extraction function. Below are vectors produced by 9-cell, 3-cell, and single-cell functions. Since these plots are of amplitude versus pixel index, the difference in resolution is apparent, the x-axis (RA) vector having 255 elements while the y-axis (Dec) vector has only 90. For the present work, the extraction function was chosen manually, however it would be possible to code a function to match the seeing conditions of the image with an appropriate circular or Gaussian binning function. For example, if the average PSF FWHM as determined from the background stars is 5", and the pixel size is 1", then the 'preferred' binning size would be a 5x5 pixel bin, weighted appropriately.

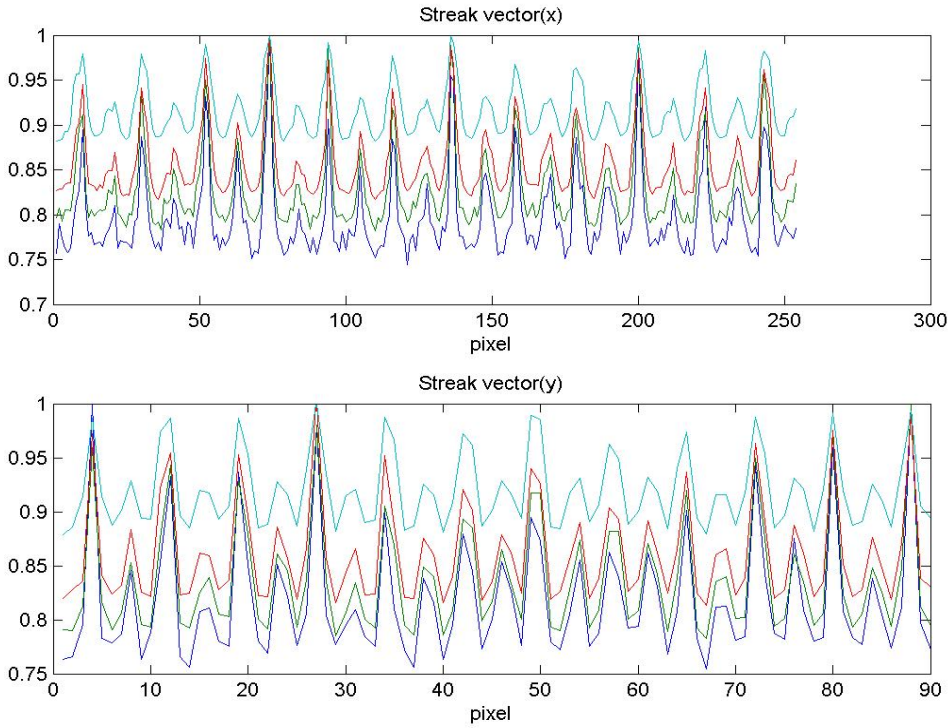


Fig. 3. Streak Vectors extracted from image of SSN#20813, Molniya 3-39. Image acquired on 2000 June 27, 2:18 UTC, 40 second exposure.

As initially generated by the SSTAS program, the individual elements of the light-curve vectors contain the actual CCD counts or sums of CCD counts along the streak. While this CCD count information may be useful for differential photometry, information in the frequency domain is the focus of this exercise. Therefore, prior to the frequency analysis the light-curve vectors are reduced by background subtraction and normalized. The vectors are initially indexed by pixel length, but, as shown below in Fig. 4, they are also indexed in time, corresponding to elapsed intervals adding up to the total CCD exposure duration. Uniform motion is assumed between the endpoints.

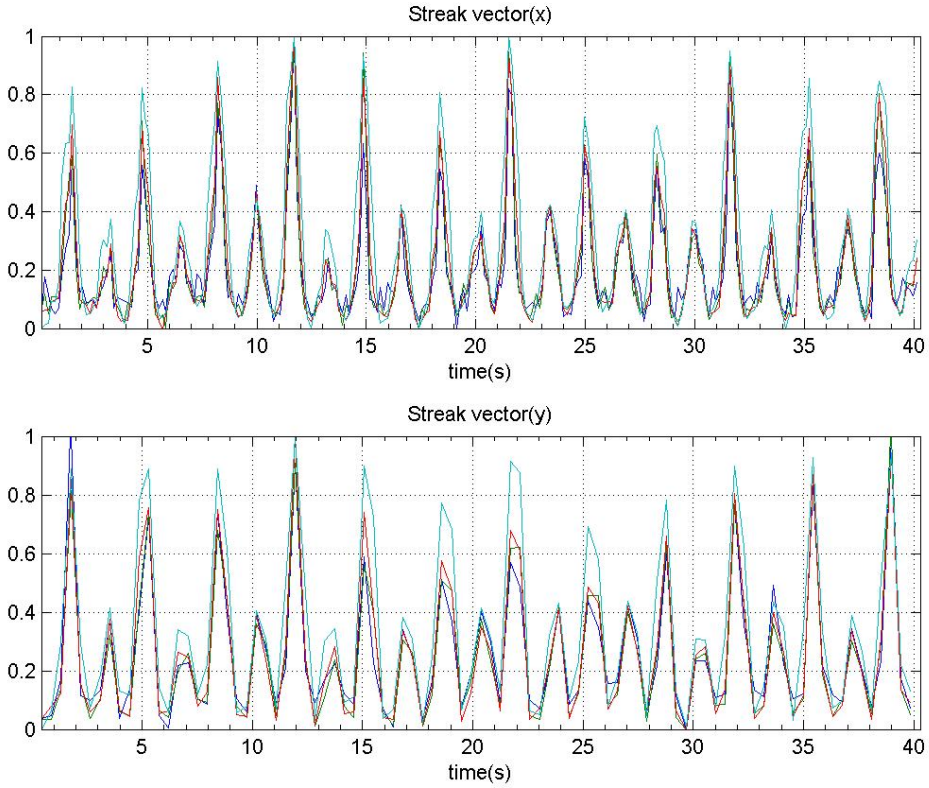


Fig. 4. Streak Vectors extracted from image of SSN#20813, Molniya 3-39. Image acquired on 2000 June 27, 2:18 UTC, 40 second exposure. Normalized amplitude versus time.

## 4. FOURIER ANALYSIS OF STREAK VECTORS

For 'clean' streaks with a high S/N ratio, a fairly simple peak-counting algorithm might be a reasonable approach to measuring the 'dominant' periodicity. This method would, however, disregard much time domain information in the streak and is difficult to apply to data when there is significant noise. Fourier transform algorithms are commonly used to find the frequency components buried in noisy time domain signals. Even in the normalized form shown in Fig. 4, however, the light-curve vectors are ill-suited for frequency analysis by Fourier decomposition. Since the vector amplitudes at the endpoints are not generally equal in amplitude, the Fourier transform algorithm produces 'edge effects'. (This follows because the transform algorithm treats the input vectors as infinite discretely sampled periodic signals.) In addition to normalization, the vectors are 'windowed' by scaling the element magnitudes by a weighting function. A Hann window was used for this analysis.[2] This weighting function has the effect of minimizing the Fourier transform frequency domain components that result from the mismatch of the streak vectors at the endpoints - the range of which is up to 100% of the signal. Windowing the vectors can introduce false components into the frequency domain, but any long-period components are discounted from our results due to the limits of the optics and camera combination. Comparisons of the results of using windowed and non-windowed vectors showed that windowing reduced the 'noise' in the frequency domain spectra.

The Fourier analysis was performed at a minimum of two resolutions. For the first Fourier analysis, the transform had the same number of basis elements as the given streak vector. The Fourier transform function uses the Cooley-Tukey decomposition algorithm [3, 4], allowing for arbitrary selection of the number of basis elements. The streak vectors were also zero-padded to the next-largest power-of-two or greater number of elements for increased resolution (but concordant loss of spectral amplitudes). Fig. 5 shows an example of the normalized frequency domain output of the script, plotted from the 'DC offset' component at 0Hz, to 1 Hz. The dominant frequency of 0.154 Hz corresponds to a period of 6.49 seconds.

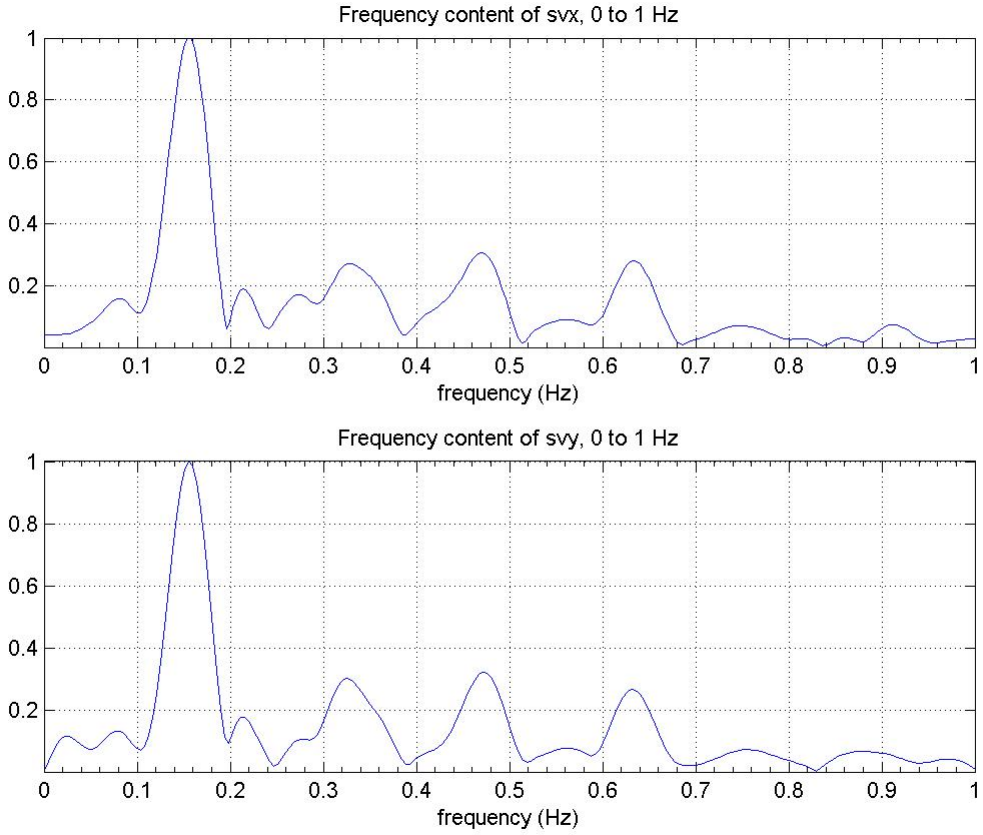


Fig. 5. Example Fourier (frequency domain) plot (normalized). From an image of SSN#12156, Molniya 1-49, acquired on 2006 July 19, 3:17 UTC.

The complete transform array (only a part of which is shown in Fig. 5) represents the frequency content of the streak in the range from 0 Hz up to the pixel-based Nyquist sampling frequency. After calling the Fourier transform function and returning the spectra of frequencies for each streak, the script calls a 'peak-finder' function in order to construct arrays of peak frequencies and relative amplitudes.

## 5. THEORY OF ATTITUDE DRIFT AND INTERPRETATION OF RESULTS

A perfectly rigid body, in the absence of applied torque, would have an angular momentum vector constant in direction and magnitude. Any rotations about the three principle spatial axes would be constant in direction and angular frequency. However, if a more realistic case is considered, then rotations about principle axes are not necessarily constant. For an elastic body, damped deformations will take place, resulting in the exchange of kinetic energy between the rotational axes of the object.[5] Of course, there may actually be applied torques - solar radiation pressure, atmospheric drag, and venting or gyroscope spin-down. In general, the light-curves of rotating space objects are intractably complex; however, one may consider some basic dynamics in order to interpret some of the common features.

For any given spin attitude, over short time periods, and in the absence of other effects such as changing illumination phase, we would expect to see at most three periodicities corresponding to specular reflections from the object as it rotates about its three spatial axes. However, these periods may lie outside the resolution of the technique applied here. For extremely short-period variations our technique is limited by the resolution of the Fourier transform for any given image or set of images – that is, fast reflection cycles cannot be discriminated. For extremely long period objects, the technique runs up against the limits imposed by the image exposure duration.

In the long term however, objects such as the Molniya-class satellites will tend to spin with most of their angular momentum vector lying on the axis of greatest moment of inertia. Perturbations on the axes of smaller moments are unstable and will tend to be transferred, while perturbations on the on the axis of greatest moment are stable.[5] For a roughly cylindrical object such as a Molniya, this means that the rotation would tend to be on an axis perpendicular to the long axis of the cylinder: that is, end-over-end rotation.

## 7. RESULTS

No conclusions about the rotational attitude of the RSOs are made here. The objects are merely characterized by the three most prominent frequencies in their Fourier transforms. From the time domain output of the SSTAS script we can construct periodicity diagrams such as Fig. 6. These circle plots display a set of observations against period, with the time domain data indicated by circles whose radii are proportional to the magnitude of the Fourier component found at the corresponding frequency. For almost all of the images in the Fig. 6 sample there is a similar dominant (primary) periodic component. For the images of 2000, the primary period is approximately 5.7 seconds, for the images of 2006, it is approximately 6.4 seconds. Secondary and tertiary components are also plotted.

Interpretation of most of the time domain spectra was straightforward, as a prominent frequency was found. The reductions on some images of SSN# 20813 and 11057 produced strong frequency components at twice the frequency seen in other images of the same objects. In such cases, we have interpreted the frequency-doubling as due to a physical symmetry in the RSO itself, causing half-cycle reflections that are intermediate to the complete cycle. Note that each image provides two determinations of the periodicity of the object. The reductions of most of the images in our data set produced nearly the same periodicities for each axis. These were averaged in our results. In the cases were the periodicities did not agree, we chose the axis with the largest resolution.

The main problem with applying this technique is the effects of bad seeing; atmospheric turbulence can induce false signals by distorting the light paths to the detector CCD. There is also the additional difficulty of disentangling optical and camera artifacts from actual signal. We have ignored the periodic components that are equal to or larger than ½ of the exposure durations of the images. These long-period signal components may be easily confused with non-signal artifacts such central image 'blooming' caused by off-axis light in the OTA, or along-track variations in atmospheric seeing conditions.

The results of the analysis are summarized in Table 1, and Fig. 7.

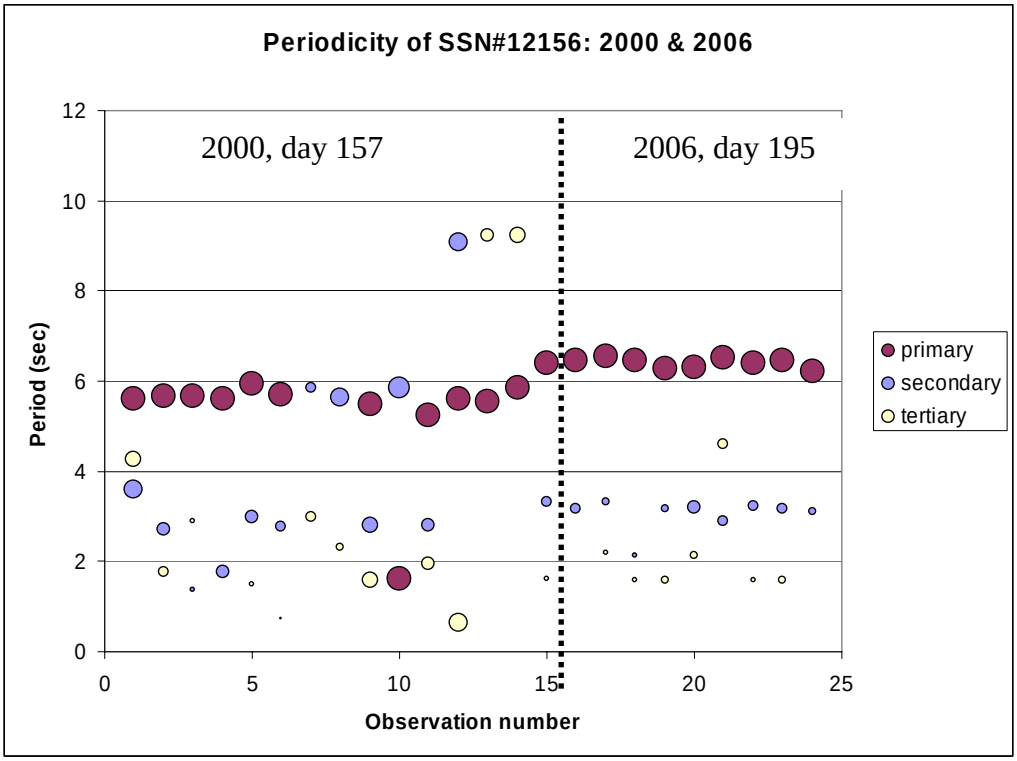


Fig. 6 - Example Fourier (frequency domain) component plot. The plot shows the three most prominent Fourier components for 24 observations of SSN#12156 (Molniya 1-49) from 2000 and 2006.

| Date | SSN# (# of Obervations) | Period (sec) |
|---|---|---|
| 2000.342 | 20813 (6) | 3.53 ± 0.19 |
| 2000.430 | 20813 (3) | 3.49 ± 0.20 |
| 2000.488 | 20813 (3) | 3.37 ± 0.20 |
| 2006.512 | 20813 (17) | 3.79 ± 0.18 |
| | | |
| 2000.430 | 12156 (24) | 5.63 ± 0.12 |
| 2006.532 | 12156 (11) | 6.41 ± 0.11 |
| | | |
| 2000.427 | 07376 (5) | 20.75 ± 0.55 |
| 2000.430 | 07376 (5) | 20.75 ± 0.55 |
| 2006.589 | 07376 (10) | 19.33 ± 0.48 |
| | | |
| 2000.093 | 11057 (3) | 10.62 ± 0.22 |
| 2000.181 | 11057 (3) | 10.51 ± 0.60 |
| 2001.017 | 11057 (10) | 11.12 ± 0.50 |
| 2006.592 | 11057 (8) | 12.70 ± 0.46 |

Table 1. Primary Periodicities of Molniyas from 2000, 2001, and 2006.

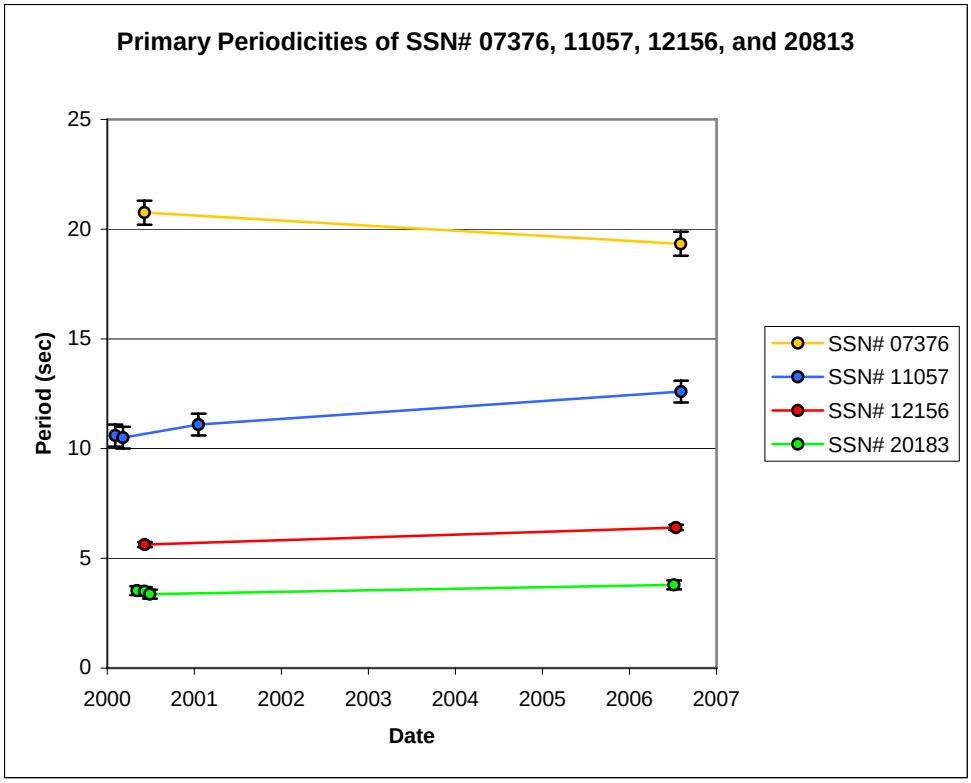


Fig. 7 - Periodicity plot of Molniyas. The plot shows the most prominent Fourier components for 108 observations of four Molniyas from 2000 to 2006.

## 8. CONCLUSIONS

The results of our study show that the periodic brightness variations of the objects we have examined remained relatively constant even over periods on the order of five years. From the rather limited data-set, we can see that this conclusion applies to SSN# 07376, 11057, 12156, and 20183. While reductions performed on some images showed intermediate periodicities, it was assumed that these are due to space-object symmetries, and the higher of the two periodicities was chosen.

The implementation of the method used here involved manual streak endpoint estimation and manual selection of the extraction algorithm. Future work will focus on further automating the reductions so that the implementation is more consistent and can easily be applied to large data sets.

## 9. ACKNOWLEDGMENTS

We wish to thank Ms. Joanna Sigaran, Capt. Paul Maskell, and Lcol. Doug Burrell for kind assistance, and also Mr. Michael Earl for his contributions in the early phases of the CD.

## 10. REFERENCES

1. Scott, R.L. and Bennett, B., “Canadian Surveillance of Space Concept Demonstrator: Metric Accuracy and Limiting Magnitude Assessment”, *Acta Astronautica* 57 (2005), pp. 302-311.

2. Oppenheim, A.V., and R.W. Schafer, *Discrete-Time Signal Processing*, Prentice-Hall, 1989, pp. 447-448.

3. Cooley, J. W. and J. W. Tukey, "An Algorithm for the Machine Computation of the Complex Fourier Series," *Mathematics of Computation*, Vol. 19 (1965), pp. 297-301.

4. Duhamel, P. and M. Vetterli, "Fast Fourier Transforms: A Tutorial Review and a State of the Art," *Signal Processing*, Vol. 19, (1990), pp. 259-299.

5. Thomson, W., *Introduction to Space Dynamics*, General Publishing Company, Toronto, 1986, pp. 212- 214.